# Investigation of analytical beam and annular plate models for automotive disc brake vibration

**D Boennen** and **S J Walsh**
Department of Aeronautical and Automotive Engineering, Loughborough University, UK

## ABSTRACT

In this paper two analytical models of automotive disc brake vibration will be presented and compared to experimental measurements. The first model approximates the brake disc as a simple beam structure with cyclo-symmetric boundary conditions. Since the beam model is a one-dimensional approach and, therefore, the modelling of the inner boundary conditions of the brake disc is impossible, a second model based upon Kirchhoff's plate theory is also presented. The mode shapes and natural frequencies of a static disc with different inner boundary conditions are calculated and compared to experimental vibration and sound pressure measurements of a brake disc made upon a static test rig. Additionally, a set of initial measurements made upon a spinning disc rig are also discussed.

## NOTATION

| | |
|---|---|
| $a$, $b$ | inner/ outer radius of the plate |
| $A$ | cross-sectional area |
| $A_i$ | amplitudes of wave component in beam model/ spinning disc model |
| $A$, $B$, $C$, $D^*$ | amplitudes of Bessel functions of plate model |
| $A^*$, $B^*$, $C^*$, $D^{**}$ | amplitudes of Bessel functions of plate model |
| $dU$ | length of a tiny element of the central hat |
| $D$ | flexural rigidity |
| $E$ | Young's modulus |
| $f_s$ | spring force per unit length |
| $h$ | thickness of the disc |
| $I$ | moment of inertia |
| $I_n$, $K_n$ | modified Bessel functions |
| $J_n$, $Y_n$ | Bessel function of the first and second kind |
| $k$ | wavenumber |

| | |
|---|---|
| $k_S$ | equivalent spring stiffness per unit length |
| $L$ | half of the length of the beam |
| $L_0$ | height of the hat of the disc |
| $M_r$ | moment |
| $n$ | mode number |
| $Q$ | shear force |
| $r$ | radius |
| $r_{i1}$, $r_{i2}$ | inner/ outer radius of brake disc hat |
| $t$ | time |
| $u$ | displacement |
| $V_r$ | Kelvin-Kirchhoff edge condition |
| $x$ | distance in x-direction along beam |
| $\alpha$ | spatial phase angle |
| $\mu$ | coefficient of friction |
| $\nu$ | Poisson's ratio |
| $\theta$ | disc angle |
| $\rho$ | density |
| $\tau$ | temporal phase angle |
| $\omega$ | circular frequency |

## 1 INTRODUCTION

Brake squeal is a phenomenon that after many years of research is still not wholly understood. So far the automotive industry has spent a huge amount of money developing and applying new processes, like the Finite Element Method (FEM) and optical measurement techniques (e.g. Electronic Speckle Pattern Interferometry (ESPI)) to identify and analyse brake squeal. In the published literature brake squeal is defined in different frequency ranges, however, a frequency range of 1000 Hz and above is generally accepted (1). Because of its large flat surface, the brake disc acts as an efficient radiator of sound and is, therefore, seen as one of the main areas in NVH development work. The two biggest problems in analysing brake squeal are its fugitive nature as well as the difficulties in its repeatability. Altering operation conditions like temperature, brake pressure and coefficient of friction can result in different squeal propensities of the brake system (2). So far there is no general agreement on what mechanism causes brake squeal, therefore many different mechanisms have been developed and discussed. Beside FEM, optical measurements and experimental testing investigations several mathematical models for the analysis of brake squeal can be found in the literature. For the beam model of brake disc vibration of the present paper the most relevant papers are from Flint and Hulten (3), who present in their papers a beam model with cyclo-symmetric boundary conditions and an assumed mode solution. A model for the transverse vibration of annular plates is presented amongst others by Leissa (4). Ouyang et al. (5) recently used the plate theory in combination with a FE model. The vibrations of the brake disc are treated as a moving load problem and the assumption has been made that the inner boundary condition of the brake disc is clamped. In contrast to the moving load problem Iwan and Moeller (6) analysed the disc vibrations using a rotating disc with a stationary transverse load. Using simpler models to analyse the vibrations of a rotating disc, Talbot and Fieldhouse (7) suggest a rotating disc mode, which can be modelled as a superposition of a forward and a backward travelling wave. In contrast, Reeves et al. (8) suggest a complex mode behaviour, which indicates the occurrence of two modes at the same frequency with a spatial and temporal

phase shift. In the present paper, beam and annular plate vibration models are developed and compared to measurement results of two static rings, two static brake discs and a spinning brake disc. In Section 2 a beam model with cyclo-symmetric boundary conditions is solved explicitly to predict the vibrational response at any point of the beam. Also presented in Section 2 is an annular plate model with a free outer boundary and either a free, simply supported, clamped or spring supported inner boundary. Additional to that, in Section 2 the complex mode solution by Reeves et al. (8) is explained and extended using the plate theory mentioned above. The experimental apparatus used for the measurements of ring and brake disc vibration are described in Section 3. In Section 4 measurement results are compared with predictions from the analytical models. Finally in Section 5 conclusions are drawn regarding the appropriateness of the developed models.

## 2 THEORY

### 2.1 Beam model

In this section the Euler-Bernoulli theory of beam bending is applied to develop a beam model of disc vibration using a wave based approach. In this approach the brake disc is modelled as a ring, which is assumed to be unwrapped into a straight beam with cyclo-symmetric boundary conditions at each end. The derivation below follows the approach of Flint and Hulten (3). However, unlike reference (3), the boundary conditions at the ends of the beam are solved explicitly to obtain the amplitudes of the constituent waves in the vibration.

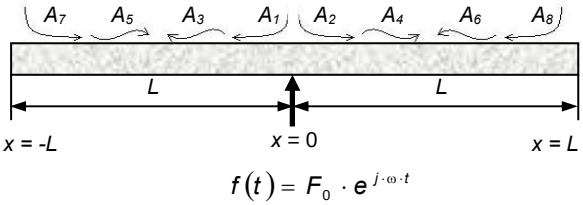


**Fig. 1 Beam model**

Consider the straight beam of finite length $2L$ excited by a force at the point $x = 0$ as shown in Fig. 1. $A_1$ and $A_2$ represent the amplitudes of the evanescent waves (near field waves) near to the force and $A_3$ and $A_4$ represent the amplitudes of the propagating waves, which travel away from the forced excitation. Cyclo-symmetric boundary conditions at the ends imply that the coefficients $A_5$, $A_6$, $A_7$ and $A_8$ represent the amplitudes $A_1$, $A_2$, $A_3$ and $A_4$, respectively, continuing beyond the boundaries. The equation of motion is given by

$$\frac{\partial^2}{\partial x^2}\cdot\left[E\cdot I\cdot\left(\frac{\partial^2 u(x,t)}{\partial x^2}\right)\right]+\rho\cdot A\cdot\frac{\partial^2 u(x,t)}{\partial t^2}=f(t) \tag{1}$$

The solution of the matrix system of equations of the boundary conditions yield the following wave amplitude relationships

$$A_1 = A_2 = -\frac{F_0\cdot e^{k\cdot L}}{4\cdot E\cdot I\cdot k^3\cdot\left(e^{k\cdot L}-e^{-k\cdot L}\right)} \qquad A_7 = A_8 = -\frac{F_0\cdot e^{-k\cdot L}}{4\cdot E\cdot I\cdot k^3\cdot\left(e^{k\cdot L}-e^{-k\cdot L}\right)}$$

$$A_3 = A_4 = -j\cdot\frac{F_0}{4\cdot E\cdot I\cdot k^3}\cdot\frac{e^{j\cdot k\cdot L}}{\left(e^{j\cdot k\cdot L}-e^{-j\cdot k\cdot L}\right)} \qquad A_5 = A_6 = -j\cdot\frac{F_0}{4\cdot E\cdot I\cdot k^3}\cdot\frac{e^{-j\cdot k\cdot L}}{\left(e^{j\cdot k\cdot L}-e^{-j\cdot k\cdot L}\right)}$$

which, as expected, show a symmetry of wave motion around the excitation location, $x = 0$.

## 2.2 Annular plate model

The scope of this section is to develop an analytical model for a non-vented brake disc by using annular plate theory. Different cases for the inside boundary are investigated: (i) free; (ii) simply supported; (iii) clamped; and (iv) spring supported. In all cases the outer boundary is assumed to be free. For the disc model *a* and *b* are the inner and outer radii and the thickness is stated as *h*. The differential equation of motion governing the displacement $u(r,\theta,t)$ of a point along the central plane of the plate can be written in the form

$$D \cdot \nabla^4 \cdot u(r,\theta,t) + \rho \cdot h \cdot \frac{\partial^2 u(r,\theta,t)}{\partial t^2} = 0 \tag{2}$$

The following solution can be assumed for a given mode, n

$$u(r,\theta) = \left(A \cdot J_n(kr) + B \cdot Y_n(kr) + C \cdot I_n(kr) + D^* \cdot K_n(kr)\right) \cdot \cos(n \cdot \theta) \tag{3}$$

### *2.2.1 Standard boundaries*

Typical boundary conditions assumed by previous authors are listed in Table 1. These boundary conditions are used in conjunction with equations (2) and (3) to predict the displacement at any point of the disc.

**Table 1 Standard boundary conditions for brake disc model**

| | **Free - free** | **Simply supported – free** | **Clamped free** |
|---|---|---|---|
| **inner boundary, r = a** | $M_r(a,\theta,t) = 0$ | $u(a,\theta,t) = 0$ | $u(a,\theta,t) = 0$ |
| | $V_r(a,\theta,t) = 0$ | $M_r(a,\theta,t) = 0$ | $\frac{\partial u(a,\theta,t)}{\partial r} = 0$ |
| **outer boundary, r = b** | $M_r(b,\theta,t) = 0$ | | |
| | $V_r(b,\theta,t) = 0$ | | |

### *2.2.2 Spring supported-free*

In the following section it is assumed that the hat is modelled out of springs with an equivalent stiffness relating to the hat's geometry and its Young's modulus. Therefore, at the inner boundary of the disc the spring force is assumed to act as a distributed force per unit length along a small element of the circumference of length *dU*, and, hence, to be equal to the Kelvin-Kirchhoff edge condition acting along the same element. $V_r(r,\theta,t)$ is defined as force per unit length parallel to the circumferential direction, $\theta$, (9). Thus,

$$f_s(r,\theta,t) \cdot dU = V_r(r,\theta,t) \cdot dU \tag{4}$$

with the spring force per unit length given by

$$f_s(r,\theta,t) = k_s \cdot u(r,\theta,t) \tag{5}$$

By applying Hook's law to a small element of length *dU* along the circumference of the cylindrical wall of the central hat the following equation can be derived

$$u(r,\theta,t) = \frac{f_s(r,\theta,t) \cdot dU \cdot L_0}{E \cdot A} \tag{6}$$

with the cross-sectional area, A, of the small element of the cylindrical wall of the hat approximated by rectangular dimensions

$$A = dU \cdot (r_{i2} - r_{i1}) \tag{7}$$

where, $r_{i2}$ is defined as the outer radius and $r_{i1}$ as the inner radius of the hat. By using equations (5)-(7) an expression for the spring stiffness per unit length can be found as

$$k_S = \frac{E \cdot (r_{i2} - r_{i1})}{L_0} \tag{8}$$

Substituting equation (8) into equation (4) leads to the following boundary condition at the inner edge of the disc,

$$V_r(r,\theta,t) - u(r,\theta,t) \cdot \frac{E \cdot (r_{i2} - r_{i1})}{L_0} = 0 \tag{9}$$

Note that the inner radius of the disc, $r = a$, is the same as the inner radius of the hat, $r = r_{i1}$. For the second inner boundary condition the bending moment in radial direction is assumed to be zero.

### 2.3 Spinning disc model

Reeves et al. (8) describe the vibration of a spinning disc using two different kinds of vibration modes: a complex mode which consists of two modes at the same frequency with a spatial and temporal phase shift; and a standing mode, which is defined as a special case of the complex mode with just one mode excited. The surface vibration of a complex mode is described in reference (8) as

$$u(\theta,t) = A_1 \sin(\omega \cdot t + \tau_1) \cdot \sin(n \cdot \theta + \alpha_1) + A_2 \sin(\omega \cdot t + \tau_2) \cdot \sin(n \cdot \theta + \alpha_2) \tag{10}$$

The variables in the case of a complex mode are set to

$$A_1 = A_2, \qquad 0 < |\tau_1 - \tau_2| < \pi/2, \qquad 0 < |\alpha_1 - \alpha_2| < \pi/2$$

and for the case of the pure standing mode, which would be the case for a static disc, to

$$A_1 = A_2, \qquad \tau_1 = \tau_2, \qquad \alpha_1 = \alpha_2$$

It was noted in reference (8) that different combinations of the variable values can yield similar results to the variables above. For the current analysis, since in both cases $A_1$ is equal to $A_2$, it is assumed that both can be substituted by the radial dependence expression of equation (3). Further a cosine function is used to represent the circumferential modes so as to be in accordance to plate theory mentioned above. Thus,

$$\begin{aligned} u(r,\theta,t) = &\left(A \cdot J_n(kr) + B \cdot Y_n(kr) + C \cdot I_n(kr) + D^* \cdot K_n(kr)\right) \cdot \\ &\left(\sin(\omega \cdot t + \tau_1) \cdot \cos(n \cdot \theta + \alpha_1) + \sin(\omega \cdot t + \tau_2) \cdot \cos(n \cdot \theta + \alpha_2)\right) \end{aligned} \tag{11}$$

For the static disc and the spinning disc case the influences of the excitation mechanism have not yet been investigated. An idealised structure with one-point excitation is assumed, which

means the effects of the brake pads are ignored. Therefore, the static case could be explained as a backward and a forward travelling wave, which when superimposed result in a standing mode pattern. In the spinning case for an observer fixed in space the wave speeds of these waves appear changed due to the effect of rotation (1). To simplify the analyses $|\tau_1 - \tau_2|$ is taken to be equal to $|\alpha_1 - \alpha_2|$.

## 3 EXPERIMENTAL APPARATUS AND METHOD

To verify the predictions made from the model described in Section 2 measurements were made of the vibrational behaviour of a number of test structures. The dimensions and material properties of the test structures are listed in Table 2.

**Table 2 Dimensions and material properties of the experimental test structures.**

| Test structure | E /N/m$^2$ | ρ /kg/m$^3$ | ν | ø$_{outside}$ /mm | ø$_{inside}$ /mm | h /mm |
|---|---|---|---|---|---|---|
| **ring** | $2.1 \cdot 10^{11}$ | 7850 | 0.3 | 950 | 850 | 5 |
| **annular plate** | $1.2 \cdot 10^{11}$ | 7250 | 0.26 | 262.3 | 160 | 14 |
| **brake disc** | $1.2 \cdot 10^{11}$ | 7250 | 0.26 | 262.3 | 152/140 excluding/including contact area with hat | 14 |

### 3.1 Experimental steel ring

In order to validate the cyclo-symmetric beam model, Frequency Response Function (FRF) measurements were conducted on a large diameter steel ring shown in Fig. 2. The ring was suspended vertically with thin wires from a large frame and excited by an electrodynamic over the frequency range of 0-3200 Hz. The vibrational response of the ring was measured by placing an accelerometer at excitation location and then at equidistant positions around the ring.

**Fig. 2 Steel ring**

### 3.2 Annular plate

In order to validate the free-free annular plate model presented in Section 2.2 FRF measurements were made on an annular plate formed from a brake disc with its central hat removed. The dimensions and material properties of the annular plate are given in Table 2. The FRF measurements were made by measuring the applied force and resonance acceleration at the excitation location.

### 3.3 Brake disc

*3.3.1 Static disc measurements*

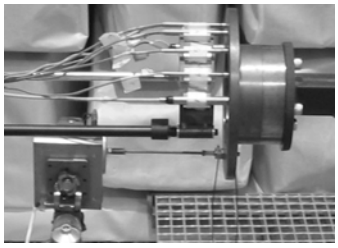

**Fig. 3 Static brake disc**

In order to compare the simply supported-free, clamped-free and spring supported-free annular plate models with experimental measurements, a brake disc was attached to a rigid frame. FRF measurements, using a force transducer attached to an electrodynamic exciter and an accelerometer, were made at 32 locations around the disc circumference. To identify displacement patterns in the radial direction a number accelerometer measurements were also made between the inner and outer radii of the brake disc. Additional to the accelerometer measurements a microphone array has been built up such that eight microphones have been fixed to a steel

frame at a distance of 5 mm from the disc and at 20° distance between each other as shown in Fig. 3. The mid-radius of the microphone array was about 109.5 mm. With a sampling rate of 25.6 kHz time history of sound radiation from the disc has been taken. The sound radiation is assumed to be in direct relation to the out-of-plane surface velocity of the disc (8). The disc has been excited using a sinusoidal signal at the frequency of the mode of interest.

### *3.3.2 Spinning disc measurements*

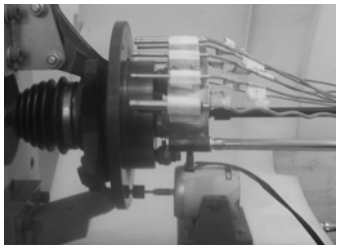

**Fig. 4 Spinning disc**

In order to validate the proposed solution from the spinning disc model of Section 2.3, microphone measurements of a spinning disc have been conducted. For the estimation of the resonant frequencies over the rpm range of interest (0-20 rpm) a single microphone has been positioned close to the disc. The spinning disc was excited with a random input using a single point excitation (Fig. 4). The single point excitation was realised by fixing a ball bearing system to an electrodynamic exciter. To identify the vibration modes the same microphone array and measurement setup as in Section 3.3.1 has been used.

## 4 RESULTS AND DISCUSSION

### 4.1 Experimental ring

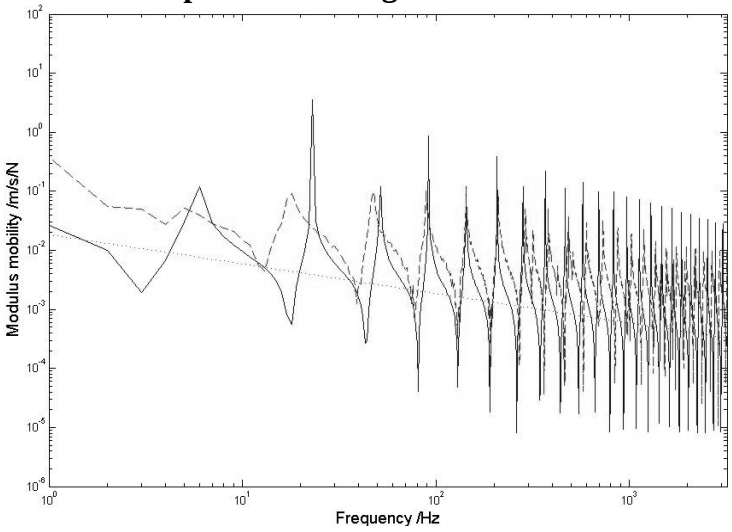


**Fig. 5 Modulus of the point mobility of the experimental steel ring**

In Fig. 5 a comparison of the modulus of the measured point mobility of the experimental ring (dashed line) with a theoretical prediction of the point mobility from the cyclo-symmetric beam model developed in Section 2.1 (solid line) over a frequency range from 1 to 3200 Hz is shown. The modulus of the point mobility of the equivalent “infinite” beam (10) (dotted line) is shown as well. It can be seen that both the theoretical prediction (solid line) and the measured data (dashed line) follow the trend of the equivalent “infinite” structure, thus, indicating beam-like behaviour. In the mid-frequency region (100-500 Hz) the predicted natural frequencies of the structure correspond approximately to the measured resonant frequencies of the ring. However, above 500 Hz there is an increasing divergence between the predicted and measured values. This may be due to incorrect values of the material properties of the ring as they were obtained from standard texts. The divergence below 100 Hz can be explained by the fact that at low frequencies the effect of curvature becomes more significant (11).

### 4.2 Annular plate

The comparison of the results of the FRF measurements of the annular plate with a theoretical prediction from the cyclo-symmetric beam model shows very little agreement between them.

This is not surprising since for the annular plate the frequency when half a bending wavelength occurs between the inner and outer radii is 1217 Hz. Thus, plate-like behaviour is to be expected over most of the frequency range. An estimate of the Young's modulus of the brake disc was made by correlating the measured resonant frequencies to the analytical results of the free-free annular plate model. For the correlation, the Poison's ratio was kept constant at 0.26, which is a representative value for cast iron and the density was estimated by weighting the structure and measuring its volume, giving a result of 7250 kg/m$^3$. The Young's modulus in the theoretical model was then adjusted until an apparent "best fit" between the predicted natural frequencies and the measured resonant frequencies was obtained, giving a value of 1.2*10$^{11}$ N/m$^2$, which is a representative value for a cast iron brake disc (5).

## 4.3 Brake disc

### *4.3.1 Static disc measurements*

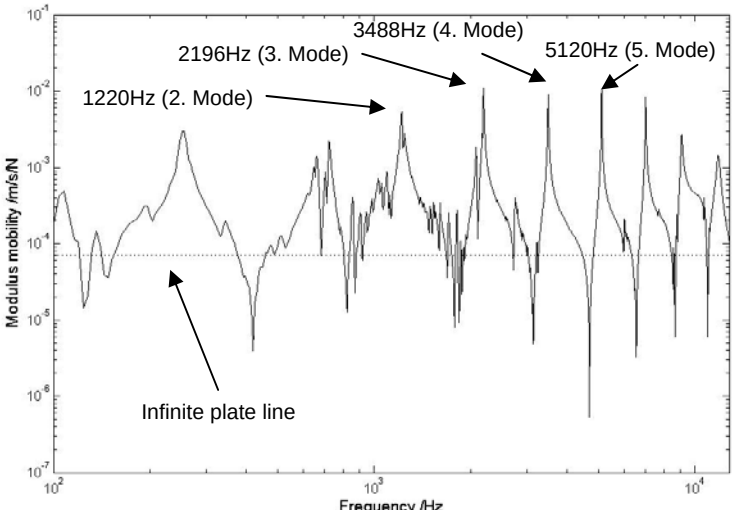


**Fig. 6 Modulus of the point mobility of the static brake disc**

In Fig. 6 the measured modulus point mobility of the static brake disc (solid line) as well as the trend line for the equivalent "infinite" plate is displayed. It can be seen that the measured point mobility follows the trend line of the equivalent "infinite" plate (dotted line). The main resonant frequencies of the brake disc are labelled in Fig. 6 and listed in Table 3. The frequencies below 1000 Hz are outside the range of interest and are, therefore, not further investigated. In the first instance the corresponding mode shapes were identified from the accelerometer measurements around the disc circumference and across its width. Additional to that the results of the microphone measurements can be used for identifying the mode shapes. In Fig.7 the theoretical prediction of the plate model, equation (11), as well as the results of the microphone measurements are displayed for the 3rd diametral mode.

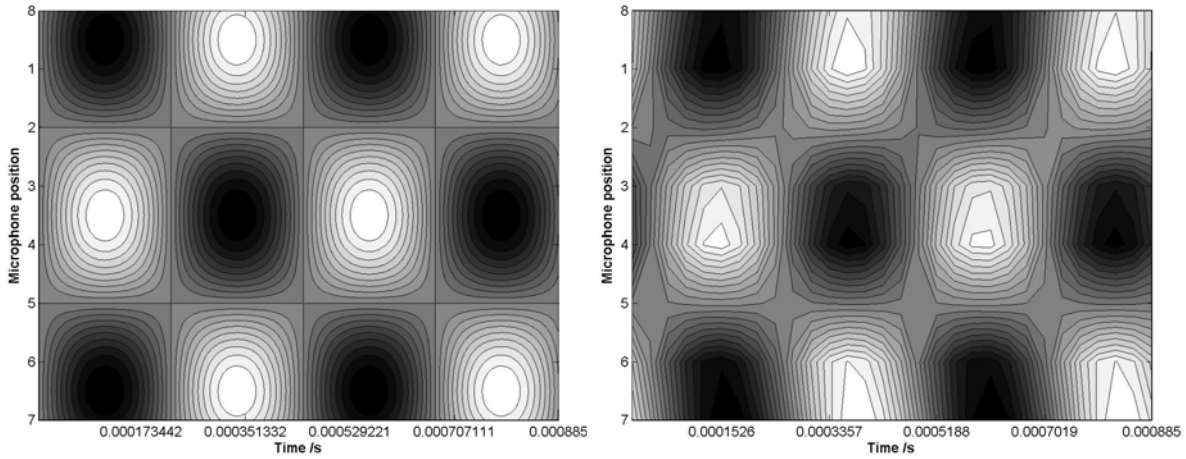


**Fig. 7 Comparison of theoretical prediction of the plate model (left) to the microphone measurements of the static disc (right), 3$^{rd}$ diametral mode**

In Table 3 it can be seen that there is a large discrepancy between the predicted clamped-free natural frequencies and the measured resonant frequencies. The comparison between the simply supported-free model and the measured resonant frequencies shows smaller differences. However, the best correlation with the measured resonant frequencies are the natural frequencies predicted by the spring supported-free disc model.

**Table 3 Comparison of the predicted natural frequencies of the annular plate with different inner boundary conditions with the measured resonant frequencies of the brake disc with 14 mm thickness.**

| Diametral mode, $n$ | Clamped, $f_{calc.}$ /Hz | Simply supported, $f_{calc.}$ /Hz | Spring supported, $f_{calc.}$ /Hz | Measured, $f_{meas.}$ /Hz |
|---|---|---|---|---|
| 2 | 3198 | 1535 | 1325 | 1220 |
| 3 | 3784 | 2520 | 2248 | 2196 |
| 4 | 4798 | 3895 | 3599 | 3508 |
| 5 | 6273 | 5655 | 5367 | 5120 |

### *4.3.2 Spinning disc measurements*

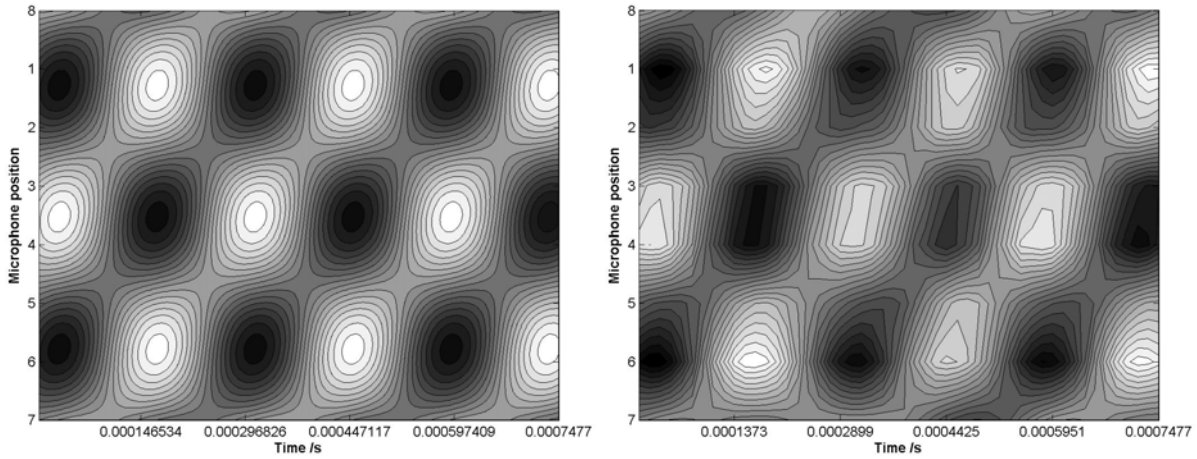


**Fig. 8 Comparison of theoretical prediction of the spinning disc model (left) to the microphone measurements of the spinning disc (right), 4$^{th}$ diametral mode, 20 rpm**

In Fig. 8 the comparison between the theoretical predictions of the spinning disc model, equation (11), and the microphone measurements of the spinning disc at 20 rpm is shown. The value used for $|\tau_1-\tau_2|$ and $|\alpha_1-\alpha_2|$ is 45°. The value was found by obtaining the "best-fit" between measurements and theoretical prediction.

## 5 SUMMARY

This paper has reported on a number of models used in the study of disc brake vibration. The following conclusions can be drawn from these investigations:

(i) in the mid-frequency range the predicted point mobility from the straight beam model with cyclo-symmetric boundary conditions showed good agreement with the measured point mobility of the experimental steel ring. At low frequencies differences between the measured and predicted data are due to the effect of curvature upon the wave motion. The discrepancies at high frequencies between predicted point mobility of the beam model and the measured point mobility of the experimental ring may have been due to inaccuracy in the assumed value of the Young's modulus of the structure.

(ii) a comparison of the predicted point mobility from the beam model with the measured mobility of the annular disc showed very little agreement. These differences were attributed to the plate-like vibrational behaviour of the annular disc.

(iii) the natural frequencies obtained by the free-free annular plate model showed good agreement with the measured resonant frequencies of the annular disc when the "best fit" value of the Young's modulus of the structure was used.

(iv) the natural frequencies, which have been predicted by the spring supported-free annular plate model, showed the best agreement with the measured resonant frequencies of the rigidly mounted brake disc. The natural frequency values predicted by the simply supported-free annular plate model gave the next closest estimates, and the clamped-free annular plate model provided the least satisfactory agreement.

(v) the results of the complex mode spinning disc model show a good correlation with the measured sound pressure distributions from the spinning disc results.

## 6 ACKNOWLEDGMENT

The authors gratefully acknowledge the support of Jaguar and Land Rover Research.

## REFERENCES

1 **Kinkaid, N.M.** Review Automotive disc brake squeal. *Journal of Sound and Vibration*, 2003, **267**, 105-166.

2 **Papinniemi, A**. Brake Squeal: a literature review. *Applied Acoustics*, 2002, **63**, 391-400.

3 **Flint, J.** and **Hulten, J**. Lining-Deformation-Induced modal coupling as squeal generator in a distributed parameter disc brake model. *Journal of Sound and Vibration*, 2002, 254, 1-21.

4 **Leissa, A.W.** Vibration of Plates. *NASA SP-160*, 1969, Ohio State University, Columbus, Ohio

5 **Ouyang, H**., **Cao, Q.**, **Mottershead, J.E.** and **Treyde, T.** Vibration and squeal of a disc brake: modelling and experimental results, *Proc. Instn. Mech. Engrs., Part D, J. of Automotive Engineering*, 2003, **217**, 867-875.

6 **Iwan, W.D.** and **Moeller, T.L.** The Stability of a Spinning Elastic Disk With a Transverse Load System, *Transaction of the ASME - Journal of Applied Mechanics*, 1976, **43**, 485-490

7 **Talbot, C. and Fieldhouse, J.D.** Graphical representation of disc brakes generating noise using data from laser holography. *Vehicle Noise and Vibration 2002*, London, 11-12 June 2002, paper C605/021/2002, pp.45-59, IMechE 2002, (Professional Engineering Publishing, Bury St Edmunds and London).

8 **Reeves, M., Taylor, N., Edwards, C., Williams, D.** and **Buckberry, C.H.** A study of brake disc modal behaviour during squeal generation using high-speed electronic speckle pattern interferometry and near-field sound pressure measurements. *Proc. Instn. Mech. Engrs., Part D, J. of Automotive Engineering*, 2000, **214**, 285-296.

9 **Wang, C.-T.** Applied Elasticty. *McGraw-Hill Book Company*,1953, ISBN 07-068125-2.

10 **Cremer L., Heckl M.** and **Unger E.E.** Structure-Borne Sound - Structural Vibrations and Sound Radiation at Audio Frequencies. *Springer-Verlag*, Berlin, 1988.

11 **Walsh, S.J**. and **White, R.G.** Mobility of a semi-infinite beam with constant curvature. *Journal of Sound and Vibration*, 1999, 221(5), 887-902.